FRACTAL MODELLING AND ANALYSIS OF FLOW-FIELD IMAGES

Pouya Dehghani Tafti[*]*, Ricard Delgado-Gonzalo*[*]*, Aurélien F. Stalder*[§‡]*, and Michael Unser*[*]

[*]Biomedical Imaging Group, Ecole Polytechnique Fédérale de Lausanne (EPFL), Switzerland
[§]Dept of Diagnostic Radiology – Medical Physics, University Hospital Freiburg, Germany
[‡]Dept of Radiology, Xuanwu Hospital, Capital Medical University, Beijing, China

ABSTRACT

We introduce stochastic models for flow fields with parameters that dictate the scale-dependent (self-similar) character of the field and control the balance between its rotational vs compressive behaviour. The development of our models is motivated by the availability of imaging modalities that measure flow vector fields (flow-sensitive MRI and Doppler ultrasound). To study such data, we formulate estimators of the model parameters, and use them to quantify the Hurst exponent and directional properties of synthetic and real-world flow fields (measured by means of phase-contrast MRI) in 3D.

***Index Terms*—** vector fractional Brownian motion, flow-sensitive MRI, wavelets, vector fields, Hurst exponent, curl, divergence.

1. INTRODUCTION

Stochastic fractal models are commonly used in a range of applications where some form of self-similarity or scale-invariance is observed (examples include image processing, seismology, and the study of growth processes [1, 2]). The quintessential stochastic fractal is the fractional Brownian motion (fBm)—so named by Mandelbrot and Van Ness [3] but already considered by Kolmogorov [4] and others before them—which can be defined by means of the structure of its variogram (variance of increments) [5]:

$$\mathbb{E}\{|B_H(\boldsymbol{x}) - B_H(\boldsymbol{y})|^2\} \propto \|\boldsymbol{x} - \boldsymbol{y}\|^{2H}$$

In the above equation $\mathbb{E}$ denotes the mathematical expectation operator; H is the Hurst exponent, named after H.E. Hurst who first used estimates of its value in the context of hydrology. The definition is not complete unless we also mention that B_H is a Gaussian process with zero mean which almost surely takes the value 0 at $\boldsymbol{x} = \boldsymbol{0}$.

Fractal behaviour is also observed in the study of flow and turbulence [6]. With the availability of new biomedical imaging techniques that allow of measurement of flow fields (e.g. Doppler ultrasound or flow-sensitive MRI [7, 8]), the question of the applicability of fractal models to these measured phenomena naturally arises. In order to address this question, it is necessary first to generalize the classical scalar fractal models to the vector setting, and then use statistical methods to compare these models against simulated and real-world data. In this paper we take steps in the mentioned directions.

To define the vector counterpart of fBm, we rely on the observation (also classical) that fBm may be regarded as the solution of a fractional differential equation involving fractional Laplacians, subject to zero boundary conditions at $\boldsymbol{x} = \boldsymbol{0}$ [9, 10]:

$$(-\Delta)^{\frac{H}{2}+\frac{d}{4}} B_H = \epsilon_H W \tag{1}$$

This work was funded by the Swiss Science Foundation under grant 200020-121763.

(d is the dimension of the domain; W is a normalized white Gaussian noise process; and ϵ_H is a proportionality constant). A vector generalization is then obtained by replacing the scalar Laplacian in (1) with a(n extended) vector Laplacian (Section 2). In addition to the Hurst exponent, the new random model is indexed by two (dependent) additional parameters that control the balance between rotational and divergent or convergent tendencies in the field.

We shall employ wavelets to address the second aspect (statistical study of the models). Wavelet-based techniques have been used with efficacy in the past in the statistical analysis of fBm and, in particular, in the estimation of the Hurst exponent [2, 10–14]. The effectiveness of wavelet analysis for this purpose relies on two facts: First, wavelets essentially behave as low-frequency differentiators, and this, by virtue of Eqn (1), means that a wavelets analysis of fBm (which is non-stationary) yields coefficients that correspond to (stationary) filtered white noise. Second, the multi-scale nature of a wavelet analysis captures the self-similar structure of fBm.

Consequently, in order to move towards understanding the connection between vector fBm models and biomedical data, in Section 3 we develop a wavelet estimator of the parameters of the model, which we then apply to synthetic fields and measured phase-contrast MRI data (Section 4). A few remarks and observations conclude the paper (Section 5).

2. VECTOR FRACTIONAL BROWNIAN MOTIONS

The vector extension of Fractional Brownian Motion (fBm) we shall consider spans a new[1] family of random vector field models that are singled out by their special invariance and self-similarity properties with respect to changes of scale and rotations of the coordinate system. These random fields can be defined as solutions of the parametric fractional differential equation (a.k.a. whitening equation)

$$(-\boldsymbol{\Delta})^{\frac{H}{2}+\frac{d}{4}}_{\boldsymbol{\xi}} \boldsymbol{B}_{H,\boldsymbol{\xi}} = \epsilon_H \boldsymbol{W} \tag{2}$$

where: $\boldsymbol{W}$ is a vector of independent white Gaussian noises; $(-\boldsymbol{\Delta})^{\gamma}_{\boldsymbol{\xi}}$ is an extended fractional Laplacian we shall define below; H denotes the Hurst exponent that is a measure of the dependence of the values of the random field at different locations; d is the number of spatial dimensions; $\boldsymbol{\xi} = (\xi_1, \xi_2)$ is a vector of (dependent) parameters that, as we shall see, capture the directional behaviour of the vector field; and ϵ_H is a special constant. The equation is to be solved by imposing zero boundary conditions at the origin.

The fractional vector Laplacian that appears in Eqn (2) is a combination of the fractional Laplacian (Riesz derivative) $(-\boldsymbol{\Delta})^{\gamma}$, defined in the Fourier domain by the symbol $\|\boldsymbol{\omega}\|^{2\gamma}$, and a rebalancing of the divergence-free and curl-free components of the

[1] To the best of the authors' knowledge.

operand, achieved by means of an operator $\mathbf{E}$ that projects its operand onto its curl-free component[2] and has Fourier symbol $\boldsymbol{\omega}\boldsymbol{\omega}^\mathsf{T}/\|\boldsymbol{\omega}\|^2$. In symbols:

$$(-\boldsymbol{\Delta})^\gamma_{\boldsymbol{\xi}} = \big[\mathrm{e}^{\xi_1}\mathbf{E} + \mathrm{e}^{\xi_2}(\mathrm{Id} - \mathbf{E})\big](-\boldsymbol{\Delta})^\gamma$$

with

$$\begin{aligned}
(-\boldsymbol{\Delta})^\gamma &\quad\overset{\mathcal{F}}{\longleftrightarrow}\quad \|\boldsymbol{\omega}\|^{2\gamma} \\
\mathbf{E} &\quad\overset{\mathcal{F}}{\longleftrightarrow}\quad \frac{\boldsymbol{\omega}\boldsymbol{\omega}^\mathsf{T}}{\|\boldsymbol{\omega}\|^2} \\
(-\boldsymbol{\Delta})^\gamma_{\boldsymbol{\xi}} &\quad\overset{\mathcal{F}}{\longleftrightarrow}\quad \|\boldsymbol{\omega}\|^{2\gamma}\Big[\mathrm{e}^{\xi_1}\frac{\boldsymbol{\omega}\boldsymbol{\omega}^\mathsf{T}}{\|\boldsymbol{\omega}\|^2} + \mathrm{e}^{\xi_2}\big(\mathbf{I} - \frac{\boldsymbol{\omega}\boldsymbol{\omega}^\mathsf{T}}{\|\boldsymbol{\omega}\|^2}\big)\Big] =: \hat{\Phi}^\gamma_{\boldsymbol{\xi}}(\boldsymbol{\omega})
\end{aligned}$$

(note the definition of the matrix valued function $\hat{\Phi}^\gamma_{\boldsymbol{\xi}}$; also note that, at least for $\gamma \geq 0$, the operators $(-\boldsymbol{\Delta})^\gamma$ and $\mathbf{E}$ commute).

The inverse of $(-\boldsymbol{\Delta})^{H/2+d/4}_{\boldsymbol{\xi}}$, taking into account the zero boundary conditions at $\boldsymbol{x} = \mathbf{0}$, is given by the integral operator

$$(-\boldsymbol{\Delta})^{-\gamma}_{-\boldsymbol{\xi}} : \boldsymbol{f} \mapsto \frac{1}{(2\pi)^d}\int_{\mathbb{R}^d}\Big(\mathrm{e}^{\mathrm{j}\langle \boldsymbol{x},\boldsymbol{\omega}\rangle} - \sum_{|\boldsymbol{k}|\leq\lfloor H\rfloor}\frac{\mathrm{j}^{|\boldsymbol{k}|}\boldsymbol{x}^{\boldsymbol{k}}\boldsymbol{\omega}^{\boldsymbol{k}}}{\boldsymbol{k}!}\Big)\cdot \hat{\Phi}^{-\gamma}_{-\boldsymbol{\xi}}(\boldsymbol{\omega})\hat{\boldsymbol{f}}(\boldsymbol{\omega})\,\mathrm{d}\boldsymbol{\omega}$$

($\hat{\boldsymbol{f}}$ denotes the distributional Fourier transform of $\boldsymbol{f}$). The following identity is easy to establish.

$$(-\boldsymbol{\Delta})^{-\gamma}_{-\boldsymbol{\xi}} = (-\boldsymbol{\Delta})^{-\gamma}_{\mathbf{0}}\big[\mathrm{e}^{-\xi_1}\mathbf{E} + \mathrm{e}^{-\xi_2}(\mathrm{Id} - \mathbf{E})\big]. \tag{3}$$

The inverse operator that we just introduced has the following self-similarity properties with respect to changes of scale and rotations:

$$(-\boldsymbol{\Delta})^{-\gamma}_{-\boldsymbol{\xi}}\{\boldsymbol{f}(\sigma^{-1}\bullet)\} = \sigma^{-2\gamma}\big((-\boldsymbol{\Delta})^{-\gamma}_{-\boldsymbol{\xi}}\boldsymbol{f}\big)(\sigma^{-1}\bullet) \quad \text{(scale-invariance)}$$

$$(-\boldsymbol{\Delta})^{-\gamma}_{-\boldsymbol{\xi}}\{\boldsymbol{\Omega}\boldsymbol{f}(\boldsymbol{\Omega}^\mathsf{T}\bullet)\} = \boldsymbol{\Omega}\big((-\boldsymbol{\Delta})^{-\gamma}_{-\boldsymbol{\xi}}\boldsymbol{f}\big)(\boldsymbol{\Omega}^\mathsf{T}\bullet) \quad \text{(rotation-invariance)}$$

($\boldsymbol{\Omega}$ denotes an arbitrary rotation matrix in $\mathbb{R}^d$).

Using the above inverse operator, we shall now give a direct definition of the extended vector fBm with parameters H and $\boldsymbol{\xi}$:[3]

$$\boldsymbol{B}_{H,\boldsymbol{\xi}} := \epsilon_H(-\boldsymbol{\Delta})^{-\frac{H}{2}-\frac{d}{4}}_{-\boldsymbol{\xi}}\boldsymbol{W}. \tag{4}$$

The scale- and rotation-invariance of the operator $(-\boldsymbol{\Delta})^{-H/2-d/4}_{-\boldsymbol{\xi}}$ and the statistical invariance of the white noise field $\boldsymbol{W}$ with respect to changes of scale and rotations together mean that the vector fBm $\boldsymbol{B}_{H,\boldsymbol{\xi}}$ is also statistically invariant with respect to scalings and rotations of the system of coordinates. One may also note that, as a consequence of the factorization relation (3), $\boldsymbol{B}_{H,\boldsymbol{\xi}}$ becomes divergence-free (respectively curl-free) as $\xi_1 - \xi_2$ (resp. $\xi_2 - \xi_1$) approaches $+\infty$.

A few examples of computer-generated two-dimensional vector fBm are given in Figure 1.

[2] The complement, $\mathrm{Id} - \mathbf{E}$, is a projection onto the divergence-free component

[3] The action of an operator on a random field finds a rigorous interpretation in the framework of the theory of generalized random processes of Gelfand and Vilenkin [15].

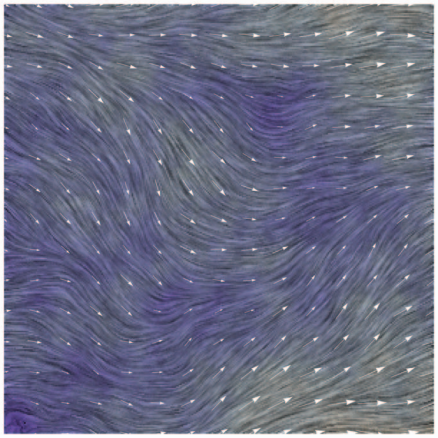

(a) $H = 0.60, \xi_1 = 0, \xi_2 = 0$

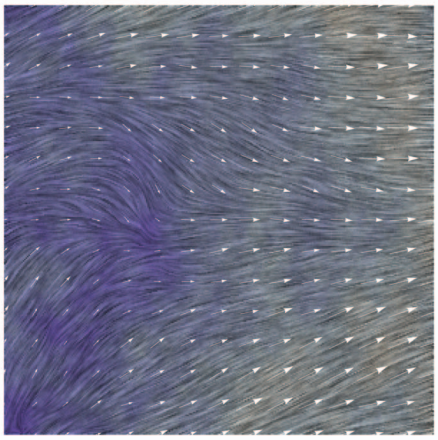

(b) $H = 0.60, \xi_1 = 0, \xi_2 = 100$

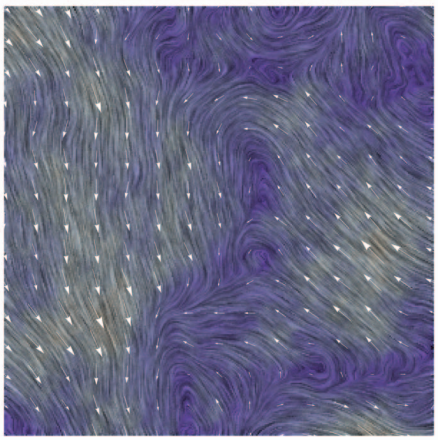

(c) $H = 0.60, \xi_1 = 100, \xi_2 = 0$

Fig. 1: Simulated vector fBm with $H = 0.6$ and variable ξ_1 and ξ_2, visualized using Mathematica's implementation of line integral convolution (LIC).

3. ESTIMATION OF VECTOR FBM PARAMETERS USING WAVELETS

It is a well-known fact that wavelet transform coefficients can be used to estimate the Hurst exponent of scalar fBm processes and fields [2, 10–14, 16]. This property of wavelets holds true also in the vector setting, in the following manner: A wavelet transform applied independently to each of the vectorial components of a fractional Brownian vector field can be used, in almost exactly the same fashion as in the scalar setting, to estimate H. We refer the reader to Tafti *& al.* [10] for the details of two such estimators.

As in the scalar case, in order for the wavelet to stationarize the random field, it has to incorporate a fractional Laplacian of sufficient order so as to cancel out the (non-shift-invariant) inverse operator in (4); which is to say that it is necessary that the mother wavelet can be written as $(-\boldsymbol{\Delta})^{\gamma}\Theta$, with $\gamma > \frac{H}{2} + \frac{d}{4}$, where Θ is a (matrix-valued) smoothing kernel. The component-wise analysis of a vector field described in the previous paragraph corresponds to the special case of Θ being a scalar matrix (i.e. a multiple of identity).

We shall now observe that such a diagonal wavelet transform is not sufficient for our purpose of estimating all parameters of a vector fBm. Indeed, while an independent component-wise analysis can provide estimates of H, such an analysis cannot differentiate between different choices of the directional parameters ξ_1 and ξ_2 in a statistically meaningful way, for the reason that it does not measure the interdependence of the vector components.

In order to estimate the directional characteristics of the field it is therefore appropriate to consider full matrix wavelets that capture the inter-component structure of the field. Such wavelets can be constructed by decomposing a scalar matrix wavelet $\Psi = (-\boldsymbol{\Delta})^{\gamma}\Theta$—where $\Theta = \theta\mathbf{I}$ is a scalar matrix function with diagonal θ—in the following fashion:

$$\begin{aligned}\Psi = (-\boldsymbol{\Delta})^{\gamma}\Theta &= (-\boldsymbol{\Delta})^{\gamma}\big[\mathbf{E} + (\mathrm{Id} - \mathbf{E})\big]\Theta \\ &= \underbrace{(-\boldsymbol{\Delta})^{\gamma}\mathbf{E}\Theta}_{\Psi_1} + \underbrace{(-\boldsymbol{\Delta})^{\gamma}(\mathrm{Id} - \mathbf{E})\Theta}_{\Psi_2}.\end{aligned}$$

Convolving Ψ_1 and Ψ_2 with $\boldsymbol{B}_{H,\boldsymbol{\xi}}$ then yields

$$\Psi_1 * \boldsymbol{B}_{H,\boldsymbol{\xi}} = \mathrm{e}^{-\xi_1}\big[(-\boldsymbol{\Delta})^{\gamma-\frac{H}{2}-\frac{d}{4}}\mathbf{E}\Theta\big] * \boldsymbol{W} =: \mathrm{e}^{-\xi_1}\boldsymbol{W}_1;$$

$$\Psi_2 * \boldsymbol{B}_{H,\boldsymbol{\xi}} = \mathrm{e}^{-\xi_2}\big[(-\boldsymbol{\Delta})^{\gamma-\frac{H}{2}-\frac{d}{4}}(\mathrm{Id} - \mathbf{E})\Theta\big] * \boldsymbol{W} =: \mathrm{e}^{-\xi_2}\boldsymbol{W}_2.$$

The random fields on the right-hand side of the above equations are stationary filtered-white-noise-type processes.

It is possible to construct a very simple estimator of the quantity $(\xi_1 - \xi_2)$ if one notes that the mathematical expectations $\mathbb{E}\{\|\boldsymbol{W}_1\|^2\}$ and $\mathbb{E}\{\|\boldsymbol{W}_2\|^2\}$ are constant functions of the spatial coordinates that depend solely on the choice of the smoothing kernel Θ.[4] The ratio

$$R := \frac{\mathbb{E}\{\|\boldsymbol{W}_1\|^2\}}{\mathbb{E}\{\|\boldsymbol{W}_2\|^2\}}$$

can therefore be pre-computed or, alternatively, estimated beforehand in a calibration step. Subsequently, for a realization of $\boldsymbol{B}_{H,\boldsymbol{\xi}}$ with unknown $\boldsymbol{\xi}$ we may estimate the ratio

$$\frac{\mathbb{E}\{\|\Psi_1 * \boldsymbol{B}_{H,\boldsymbol{\xi}}\|^2\}}{\mathbb{E}\{\|\Psi_2 * \boldsymbol{B}_{H,\boldsymbol{\xi}}\|^2\}} = \mathrm{e}^{2(\xi_2-\xi_1)}R$$

between the mean values of the energies of the two wavelet transforms; from where an estimate of $\xi_1 - \xi_2$ can be trivially obtained.

[4] Note that it is the difference of the parameters ξ_1 and ξ_2—and not their individual values as such—that determines the directional behaviour of the field.

Table 1: Estimation of the H parameter of synthesized vector fBm.

True value	average of local estimates	their variance
0.3	0.30	0.0074
0.6	0.58	0.0107
0.9	0.87	0.0140

4. EXPERIMENTS

To verify the correctness of the estimation mechanism sketched in the previous section, $64\times64\times64$ volumes of discretized vector fBm were generated in MATLAB in accordance with the synthetic model of Section 2. Estimation of the Hurst exponent was performed over local neighbourhoods, using the first of the two estimation methods described in Tafti *& al.* [10]. To obtain a finer scale progression we replaced the discrete wavelet transform of Tafti *& al.* by a Laplacian of Gaussian continuous wavelet transform with the σ parameter of the Gaussian spanning the range 0.5 to 2 with steps of size 0.25. The results are summarized in Table 1.

Next, an estimation of $\xi_1 - \xi_2$ was performed using, as input, pseudo-random realizations of vector fBm with varying $\xi_1 - \xi_2$. The estimates were fairly accurate, with the correlation coefficient being virtually equal to 1 over the range -30 to 30 with step size 2.

A similar analysis was applied to measured MRI data obtained from a phantom. We shall now briefly describe the set-up. The flow model—based on a rigid PVC tube with an inner diameter of 3.4cm—was connected to a clinical blood-pump system to produce a constant (non-pulsatile) fully developed flow. The fluid used was a solution of a Gadolinium chelate contrast agent in distilled water at 37°C. The flow model was imaged on a 3T MRI system using a 3D phase-contrast sequence [7]. The sequence relies on the difference of phase of spins moving along the direction of a magnetic field gradient to determine their velocities. The sequence, typically used for blood flow measurements in vivo [7, 8], allows the acquisition of three-directional velocities with a three-dimensional coverage. The MRI acquisition parameters were: voxel size [mm^3]: $0.4\times0.4\times0.6$, velocity encoding factor (venc) [cm/s]: 50, T E / T R [ms]: 4.62 / 8, bandwidth [Hz/pixel]: 440, flip angle (α) [degrees]: 13.

Phase-contrast MRI can assess flow velocities without restriction in anatomic coverage or direction but is limited by its relatively long imaging times, limited spatial and temporal resolutions, or limited signal to noise ratio (SNR). Errors limiting the SNR can be induced by intrinsic measurement errors, eddy currents, gradient field inhomogeneities, concomitant gradients, or acceleration errors [17].

Figure 2 schematically shows the imaging set-up, along with a colour-coded cross-section of local directional parameters $(\xi_1 - \xi_2)$; the cross-section was taken perpendicular to the direction of flow. (The significant part of the image is the circular disc on the left; the background—apart from some static structures—does not correspond to any flow and should be discarded.) A positive $\xi_1 - \xi_2$, as observed inside the tube (Figure 2b), indicates a divergence-free tendency, which is consistent with the incompressible nature of the fluid used in the experiment. Due to the non-turbulent (and essentially predictable) nature of this example, estimation of the Hurst exponent is not particularly meaningful in this case. Such an analysis would however be of great interest in studying flow fields of a more random and turbulent character. Further experiments and studies in this direction are still needed and will be the subject of our future research.

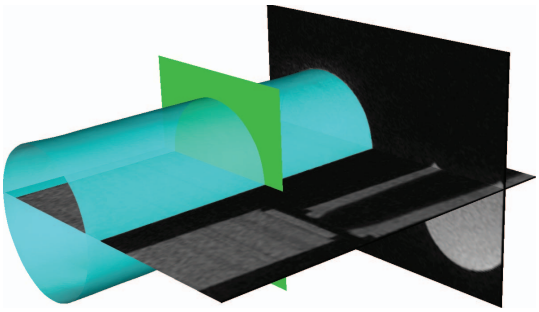

(a) Flow model (figure taken from Stalder [18])

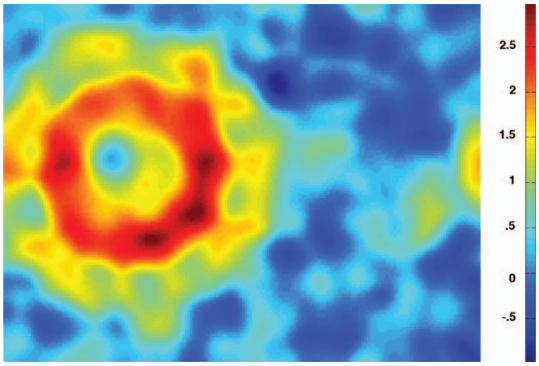

(b) Local estimates of $\xi_1 - \xi_2$

Fig. 2: Differential analysis of a 3D flow (see text for details).

5. CONCLUSION

In this paper we proposed a model for stochastic fractal vector fields in the spirit of fractional Brownian motion models that was motivated by the wish to study biomedical flow-field measurements (in particular flow-sensitive MRI data). In addition to the usual Hurst exponent that quantify the fractality of the field, the vector models we introduced also have parameters to control the balance between the extremities of irrotational and solenoidal behaviour. Next, in order to study the relevance of these models in the analysis of measured data, we developed estimators of the different parameters of these models. We verified these estimators by applying them to synthesized vector fBm, and then used them to analyze 3D flow measurements obtained using phase-contrast MRI. The outcome of the analsyis was consistent with the known properties of the flow (i.e. incompressibility). Additional experiments will be directed at a better understanding of the significance of the estimated parameters and the study of flow fields with different structures.

6. REFERENCES

[1] B. B. Mandelbrot, *The Fractal Geometry of Nature*. New York: W. H. Freeman and Company, 1982.

[2] P. D. Tafti, D. Van De Ville, and M. Unser, "Innovation modelling and wavelet analysis of fractal processes in bio-imaging," in *Proc. 5th IEEE Int. Symp. Biomed. Imaging (ISBI'08)*, (Paris, France), pp. 1501–1504, 2008.

[3] B. B. Mandelbrot and J. W. Van Ness, "Fractional Brownian motions, fractional noises and applications," *SIAM Rev.*, vol. 10, no. 4, pp. 422–437, 1968.

[4] A. N. Kolmogoroff, "Wienersche Spiralen und einige andere interessante Kurven im Hilbertschen Raum," *C. R. (Doklady) Acad. Sci. URSS*, vol. 26, no. 2, pp. 115–118, 1940.

[5] J.-P. Kahane, *Some Random Series of Functions*. Cambridge University Press, 2nd ed., 1985.

[6] M. Farge, N. Kevlahan, V. Perrier, and E. Goirand, "Wavelets and turbulence," *Proc. IEEE*, vol. 84, no. 4, pp. 639–669, 1996.

[7] M. Markl, A. Harloff, T. A. Bley, M. Zaitsev, B. Jung, E. Weigang, M. Langer, J. Hennig, and A. Frydrychowicz, "Time-resolved 3D MR velocity mapping at 3T: Improved navigator-gated assessment of vascular anatomy and blood flow," *J. Magn. Reson. Imaging*, vol. 25, no. 4, pp. 824–831, 2007.

[8] A. F. Stalder, M. F. Russe, A. Frydrychowicz, J. Bock, J. Hennig, and M.Markl, "Quantitative 2d and 3d phase contrast MRI: Optimized analysis of blood flow and vessel wall parameters," *Magn. Reson. Med.*, vol. 60, no. 5, pp. 1218–1231, 2008.

[9] A. Benassi, S. Jaffard, and D. Roux, "Elliptic gaussian random processes," *Rev. Mat. Iberoamericana*, vol. 13, no. 1, pp. 19–90, 1997.

[10] P. D. Tafti, D. Van De Ville, and M. Unser, "Invariances, Laplacian-like wavelet bases, and the whitening of fractal processes," *IEEE T. Image. Process.*, vol. 18, no. 4, pp. 698–702, 2009.

[11] S. Mallat, "A theory for multiresolution signal decomposition: The wavelet representation," *IEEE T. Pattern. Anal.*, vol. 11, no. 7, pp. 674–693, 1989.

[12] G. W. Wornell, "Wavelet-based representations for the $1/f$ family of fractal processes," *Proc. IEEE*, vol. 81, no. 10, pp. 1428–1450, 1993.

[13] D. Veitch and P. Abry, "A wavelet-based joint estimator of the parameters of long-range dependence," *IEEE T. Inform. Theory.*, vol. 45, no. 3, pp. 878–897, 1999.

[14] P. D. Tafti and M. Unser, "Self-similar random vector fields and their wavelet analysis," in *Proc. SPIE Conf. Math. Imaging: Wavelets XIII* (M. P. Vivek K. Goyal and D. V. D. Ville, eds.), vol. 7446, 74460Y, (San Diego CA, USA), pp. 74460Y–1–74460Y–8, 2009.

[15] I. M. Gel'fand and N. Vilenkin, *Applications of Harmonic Analysis*, vol. IV of *Generalized Functions*. Academic Press, 1964.

[16] R. Delgado-Gonzalo, P. D. Tafti, and M. Unser, "Fractional Laplacian pyramids," in *Proc. IEEE Int. Conf. Image Process. (ICIP 2009)*, 2009.

[17] E. Haacke, R. Brown, M. Thompson, and R. Venkatesan, *Magnetic Resonance Imaging Physics: Physical Principles and Sequence Design*. Wiley, 1999.

[18] A. F. Stalder, *Quantitative analysis of blood flow and vessel wall parameters using 4D-flow sensitive MRI*. PhD thesis, Universität Freiburg, Technische Fakultät (bisher: Fak. f. Angew. Wiss.), 2009.